International Journal of Pharmaceutics 430 (2012) 26–33

Contents lists available at SciVerse ScienceDirect

International Journal of Pharmaceutics

journal homepage: www.elsevier.com/locate/ijpharm

Influence of primary crystallisation conditions on the mechanical and interfacial properties of micronised budesonide for dry powder inhalation

Harshal A. Kubavat[a], Jagdeep Shur[a], Graham Ruecroft[b], David Hipkiss[b], Robert Price[a,*]

[a] Pharmaceutical Surface Science Research Group, Department of Pharmacy and Pharmacology, University of Bath, BA2 7AY, UK
[b] Prosonix Ltd., Magdalen Centre, Robert Robertson Avenue, Oxford Science Park, Oxford, OX4 4GA, UK

ARTICLE INFO

Article history:
Received 19 November 2011
Accepted 10 March 2012
Available online 17 March 2012

Keywords:
Dry powder inhaler
Nanoindentation
Mechanical
Atomic force microscope
Crystallisation

ABSTRACT

Investigate the influence of primary crystallisation conditions on the mechanical properties and secondary processing behaviour of budesonide for dry powder inhaler (DPI) formulations. Young's modulus of two batches of budesonide crystals (samples A and B) produced using different anti-solvents was determined using nanoindentation. Physicochemical and surface interfacial properties via the cohesive–adhesive balance (CAB) approach to colloid probe atomic force microscopy (AFM) of air-jet micronised budesonide crystals were also investigated. These data were correlated to *in vitro* aerosolization performance of carrier-based DPI formulations containing either budesonide samples A or B and lactose monohydrate. Young's modulus of budesonide samples A and B crystals was 0.95 and 4.04 GPa, respectively. Sample A crystals with low Young's modulus exhibited poorer micronisation efficiency than sample B. CAB analysis of micronised budesonide samples A and B, suggest that sample B budesonide had a greater adhesion to lactose than sample A. These data correlated with *in vitro* aerosolisation studies, which showed that the fine particle delivery of budesonide sample A was higher than that of sample B. In conclusion, crystallisation conditions may affect the mechanical properties of budesonide, and therefore secondary processing of the material and their interfacial properties and product performance in carrier based DPI formulations.

1. Introduction

The delivery of active pharmaceutical ingredient (API) to the lung via dry powder inhalers (DPI) requires the aerodynamic particle diameter of the API to be $\leq$5 μm (Newman, 2002). However, the cohesive behaviour of particles less than 10 μm has precluded efficient handling and accurate metering of the respirable dose of an API into a DPI device. As a result, the API is blended with a coarse excipient, such as lactose monohydrate, to form an adhesive mixture (Timsina et al., 1994). The structure of the formulated mixture, with respect to the formation of agglomerates and the distribution of the API on the carrier, is highly dependant on the interfacial properties of the API and the relative magnitude of the cohesive (drug–drug) and adhesive (drug–excipient) interactions (Begat et al., 2004a). The balance of these forces is dominated by the physico-chemical properties of the API, which are directly influenced by the primary and secondary processing history of the API. These inter-particulate forces also govern the resulting dispersion efficiency of the API within a DPI device (Begat et al., 2004b).

The common approach of processing APIs for lung delivery is based on a "top-down" strategy, where primary crystals from a bulk crystalliser are secondary processed using comminution techniques (*e.g.* an air-jet microniser) to reduce particle size of the API (Telko and Hickey, 2005). The particle size reduction operation is energy intensive and exerts high stresses on the input crystalline API material during particle-particle and particle-wall collisions. The result of these intense stresses is the generation of undesirable product properties such as the formation of defects and dislocations within the crystalline lattice and, at the limit, the generation of amorphous disorder (Willart and Descamps, 2008). As a result, processed particles are mechanically activated, which may adversely impact the interfacial properties and stability of the final product (Hüttenrauch et al., 1985; Brodka-Pfeiffer et al., 2003; Begat et al., 2003). However, there is limited understanding of the overall relationship between the material properties of the primary API crystals, surface interfacial properties of secondary processed micronised API particles and their impact on DPI performance.

The primary crystallisation step is utilised to isolate and purify a stable, crystal form of an API. Optimising the crystallisation conditions is critically important in obtaining the desired characteristics for manufacturability and processing of DPI products (Murnane et al., 2009). Current practices include controlling impurity levels (Wood, 2001), particle size (Beach et al., 1999) and crystal habit

* Corresponding author. Tel.: +44 0 1225 383644; fax: +44 0 1225 386114.
E-mail address: r.price@bath.ac.uk (R. Price).

0378-5173/$ – see front matter © 2012 Elsevier B.V. All rights reserved.
doi:10.1016/j.ijpharm.2012.03.020

of the primary API (Murnane et al., 2008; Abu Bakar et al., 2009). Changes to the crystal morphology of the harvested crystals are known to lead to changes in the processing behaviour of APIs, for example, during compaction of solid oral dosage forms (Garekani et al., 2001; Banga et al., 2007). An investigation into the milling performance of two different crystal habits of succinic acid suggested the crystal morphology influenced its milling behaviour (Chikhalia et al., 2006). Furthermore, changes in crystal habit have been shown to modify the interfacial properties (*e.g.* surface free energy) of the primary crystal due to modifications in the relative proportions of different chemical groups exposed on the respective growth faces. Muster and Prestidge (2002) have demonstrated the influence of molecule orientation at crystal faces on the surface free energy and interfacial interactions of model hydrophobic silica particles.

The crystallisation process has also been shown to influence the mechanical properties of primary crystals (Liao and Wiedmann, 2004), which has been reported to have a strong influence on the micronisation behaviour of solids (Zugner et al., 2006). The mechanical properties of crystalline solids can be characterised by the hardness and Young's modulus of a solid. For organic crystals, the hardness is generally low and its range small. The Young's modulus of a material represents a material's resistance to elastic deformation and has been reported to have a strong influence on the micronisation behaviour of solids (de Vegt et al., 2009) and provides a meaningful parameter to characterise possible variations in mechanical behaviour. The use of commercially available microindenters under nanoNewton loading, have been shown to observe significant differences in the elastic modulus of different pharmaceutical ingredients, which correlated well with particle size reduction efficiencies upon micronisation (Taylor et al., 2004).

The atomic force microscope (AFM) has emerged as an alternative tool in the assessment of mechanical properties of pharmaceutical materials and has enabled measurement of their Young's modulus by investigating the mechanical deformation behaviour of materials through the use of a nanoindenting probe under controlled nanoNewton loading forces (Fraxedas et al., 2002; Perkins et al., 2007). AFM nanoindentation has been successfully compared to the established microindenting approach in determining the Young's modulus of lactose monohydrate crystals (Perkins et al., 2007). This study purported the advantages of the non-destructive AFM technique as a means of accurately obtaining the Young's modulus of pharmaceutically relevant materials under Hertzian deformation. Additionally, AFM nanoindentation has been used to quantify the elastic modulus of pharmaceutical APIs including budesonide, whereby a Young's modulus of approximately 10 GPa was measured (Davies et al., 2005). A further study into different polymorphic forms of carbamazepine revealed differences in the Young's modulus of two polymorphs, which ranged from 2.69 to 5.18 GPa (Perkins et al., 2009).

The aim of the present study was to investigate the influence of crystal morphology on the mechanical properties of unprocessed API and the affect on the physicochemical and interfacial interactions of the secondary processed material including the downstream effect on carrier-based DPI formulation performance. In this study, budesonide was crystallised using two different solvents. The Young's modulus on the same crystalline {0 0 2} faces of the primary crystals of both habits was determined by AFM nano-indentation and related to the secondary processing of the materials. The interfacial properties of the secondary processed samples produced from the two different crystalline habits were determined using the cohesive–adhesive balance (CAB) approach to colloidal-probe AFM with respect to lactose monohydrate. Furthermore, the *in vitro* performance of the two samples was investigated in a carrier-based DPI formulation.

2. Methods and materials

2.1. Materials

Crystalline budesonide ($C_{25}H_{34}O_6$, molecular weight 430.534 g/mol) was supplied by (Sterling S.r.l., Perugia, Italy). Acetone, N,N-dimethylformamide and heptane were supplied by Fisher Scientific UK (Loughborough, UK) and were 99.9% pure. Ultra pure water was prepared by MilliQ from reverse osmosis (Millipore, Molsheim, France).

2.2. Methods

2.2.1. Primary crystallisation and secondary micronisation processing of budesonide

2.2.1.1. Primary crystallisation of budesonide. Primary crystals of budesonide were produced in a water-jacketed glass crystallisation vessel using a conventional solvent/anti-solvent crystallisation technique. Two different organic solvents were selected and water was used as the anti-solvent. Saturated solutions of budesonide were made using acetone (sample A) and N,N-dimethylformamide (sample B) at 25 °C followed by filtration using heated glass labware and a 0.45 μm nylon membrane filter (Whatman, Brentford, UK). Exactly 60 mL of these solutions were rapidly introduced to a sealed glass crystallisation vessel continually stirred using a magnetic stirrer at 700 rpm with water-jacket electronically maintaining the vessel temperature at 25 ± 0.1 °C (K20; Haake, Karlsruhe, Germany).

Ultra pure water was added to the vessel at a rate of 600 mL/h to obtain a ratio of 1:7 using a computer controlled syringe driver (Harvard PHD2000 Infusion Pump, Harvard Apparatus, MA, USA) connected to a hypodermic needle (21G, BD, NJ, USA). The resulting crystalline materials were extracted using vacuum filtration and washed using 100 mL cold water then dried under vacuum at 40 °C until a steady weight was achieved. Samples of these materials were then stored at 19 °C over silica gel.

2.2.1.2. Particle size reduction. Particle size reduction of the manufactured crystals of budesonide was performed using an air jet mill (McOne, Jetpharma, Balerna, Switzerland) with a feed rate of approximately 0.5 g/min using dry nitrogen gas at an operating venturi and ring pressure of 6 and 3 bar, respectively.

2.2.2. Physicochemical analysis of budesonide

2.2.2.1. Particle morphology and size analysis. Crystal and particle morphologies were determined using scanning electron microscopy (Joel, Japan) at 20 kV. Particles were attached to a carbon sticky tab and sputter coated with gold for 5 min (Edwards Sputter Coater, Crawly, UK) prior to imaging, producing a thickness of approximately 20 nm.

The particle size distribution of primary crystals and micronised samples of budesonide was measured using laser diffraction (HELOS, Sympatec, Clausthal-Zellerfeld, Germany) using a wet dispersion system (CUVETTE, Sympatec, Clausthal-Zellerfeld, Germany). Approximately 5 mg of sample was suspended in 5 mL of dispersion media, comprising of heptane (HPLC grade) and 0.1% (w/w) lecithin. The suspension was sonicated for 180 s following prior investigation ensuring no sample dissolution or destruction, before addition to a glass cuvette containing 50 mL of dispersant and a magnetic stirring bar rotating at 1000 rpm. Sizing was performed by laser diffraction over a series of 5 repeats when the optical concentration was equal to or greater than 10%, over a duration of 20 s. Particle size analysis was performed using Windox 5.0 software (Sympatec, Clausthal-Zellerfeld, Germany) to

calculate the cumulative undersize particle parameters d_{10}, d_{50}, d_{90} and the sample span.

2.2.2.2. Crystal habit modelling. Computational molecular dynamic modelling was used to predict the crystal habit for the budesonide samples (MS Modelling, Accelrrys Software Inc., Cambridge, UK). Crystallographic data for budesonide was obtained from the Cambridge Structural Database and based on single crystal diffraction data (Albertsson et al., 1978). With reference to the SEM images, the Miller indices of the crystal faces produced from the different solvent/anti-solvent combinations were identified.

2.2.2.3. X-ray powder diffraction (XRD). X-ray powder diffraction (XRD) measurements of the budesonide samples were analysed on a Bruker Powder diffractometer (D8 Advance AXS; Bruker Inc., Madison, USA). Samples were filled into 0.7 mm glass capillaries and mounted on a goniometer head. These data were collected using CuKα radiation (=1.5418 Å) over a single 2θ sweep with range of 2θ = 5–50° and step size of 0.025°/step and step time of 1.5 s. The monochromator slit was set to 2 mm.

2.2.2.4. Differential scanning calorimetry (DSC). A differential scanning calorimeter (DSC, 2190, TA Instruments, Surrey, UK) was used to perform thermal analysis on the primary crystals of budesonide after initial calibration with indium. Powder samples (n = 3) of approximately 3.0 mg were accurately weighed in aluminium pans, ensuring a total covering of the base by pressing down the samples and then hermetically sealed. The temperature was equilibrated to 50 °C before heating at a rate of 10 °C/min to 350 °C under dry nitrogen purge (0.30 L/min).

2.2.2.5. AFM nanoindentation measurements. An atomic force microscope (AFM) was used to indent (n = 9) individual crystals (n = 3) using a Nanoscope IIIa and J-scanner (all DI, Santa Barbara, CA, USA). The indenting probe was hemispherical in shape and possessed a nominally high spring constant (R150-NCL, Nanosensors, Neuchatel, Switzerland).

For accurate extrapolation of the AFM force-distance data, the true radius of the indenting tip needs to be known. Tip radius determination was performed using a tip-characterisation grating (TGT01; NT-MDT, Moscow, Russia) in which the probe being investigated is raster scanned over the test grating composed of a uniform array of sharp spikes which in turn, produces a reverse image of the probing tip. This image was deconvoluted to determine tip radius, using a well-established approach (SPIP Image Metrology ApS, Lingby, Denmark) (Hooton et al., 2004). This measurement was performed before and after indentation measurements to ensure indenting probe integrity was maintained. In this study, the hemispherical probe radius was determined to be 318 ± 48 nm. Quantification of the nominal spring constant of the cantilever was performed using a dynamic method of thermal noise analysis (Hutter and Bechhoefer, 1993). A spring constant of 36.2 ± 0.2 N/m was recorded and agreed with the manufacturers quoted value measured using the Sader method (Sader et al., 1995).

Nanoindentation measurements were performed on different areas of the {0 0 2} face of the budesonide crystals. The cantilever deflection and piezo displacement were derived into a Young's modulus value using Hertzian model of deformation shown in Eq. (1) (Hertz, 1881; Plassard et al., 2004)

$$E = \frac{3(1-\nu^2)k\Delta z}{4\delta^{3/2}R^{1/2}} \quad (1)$$

2.2.3. Cohesive–adhesive balance measurements

2.2.3.1. Topography analysis of substrate surfaces. The surface topography and roughness measurements of primary crystals of budesonide and lactose were investigated using a Nanoscope IIIa controller, a Multimode AFM and a J-type scanner (all DI, Santa Barbara, CA, USA). All AFM surface topography images were recorded in Tapping Mode operation, in which, imaging was conducted using TESP Olympus tips (Di, Cambridge, UK) at a scan rate of 1 Hz. Surface roughness measurements were analysed over a 10 μm × 10 μm area. To quantify the variations in the surface properties of the crystal surfaces, the root-mean-squared surface roughness measurement (R_q) and the mean surface roughness (R_a) of the height deviations of the surface asperities were computed using Nanoscope software (v 4.23r4, DI, Santa Barbara, CA, USA).

2.2.3.2. Colloid probe force measurements. Prior to force measurements, a random selection of particles from each micronised batch of budesonide were attached onto standard V-shaped tipless cantilevers with pre-defined spring constants (DNP-020, DI, CA, USA) using an epoxy resin glue (Araldite, Cambridge, UK), using a previously described method (Young et al., 2006). Five probes were prepared for each batch, and all probes were examined with an optical microscope (magnification 50×) to ensure the integrity of the attached particle, before and after colloid probe force measurements.

The {0 0 2} crystal faces of each crystallised sample of budesonide was used for AFM-CAB measurements as described previously (Begat et al., 2004a). The surface roughness as measured by the R_a and R_q of the surfaces of crystal particles from each primary source of budesonide samples was <1 nm and were therefore used for measuring the force of cohesion. In order to measure the force of adhesion of the secondary processed micronised budesonide, smooth surfaces of lactose was crystallised. Briefly, atomically smooth lactose crystals were generated as described elsewhere. Briefly, a solution of lactose (1 g m^{-1}) in double-distilled water was heated to 100 °C with constant stirring and, then filtered through a 0.2 μm PTFE membrane filter (Whatman Inc, Clifton, NJ, USA). A single saturated drop of the lactose solutions was administered on to the centre of a glass cover slip (Agar Scientific, Stansted, UK) and a second cover slip was placed on top to form a sandwich. The sandwich was then allowed to cool resulting in the production of large atomically smooth crystals of lactose. The process of crystallisation was monitored by optical microscopy and the cover slips carefully separated once all the solvent had evaporated, resulting in the growth of crystals over the surface of both cover slips.

Substrates were loaded on to the AFM scanner stage, which was enclosed in a custom-built environmental chamber, in which the ambient conditions were maintained at a constant temperature of 25 °C (±1.5 °C) and relative humidity of 35% RH (±3%). The interactive forces of the colloid probes with the lactose and budesonide substrates were measured by recording the deflection of the AFM cantilever as a function of the substrate displacement (z) by applying Hooke's law ($F = -kz$). Individual force curves (n = 1024) were collected over a 10 μm × 10 μm area using the force volume mode at a scan rate of 4 Hz and a compressive load of 40 nN. Parameters were kept constant over the study. In order to quantify AFM force measurements it was imperative to measure the spring constants of the cantilevers used. Quantification of the nominal spring constant of the cantilever was performed using a dynamic method of thermal noise analysis.

With the vast array of data generated during force volume measurements, custom-built software was used to extract data. These collected force data were analysed to ensure normal distribution, indicating uniform contact between the drug probe and excipient substrate. Arithmetic mean and standard deviation were obtained from force data and used to produce CAB plots for the interactions of the different processed batches of budesonide.

2.2.4. Carrier-based DPI formulation preparation and in vitro aerosolisation analysis

2.2.4.1. HPLC analysis of budesonide. Quantification of budesonide utilised a HPLC coupled with a UV detection system (Jasco PU-980, Jasco Corp., Japan). The mobile phase utilised for the detection of budesonide consisted of HPLC grade methanol (45%), acetonitrile (35%) and 20% ultra pure water. The mobile phase was pumped at a flow rate of 1.5 mL/min, through a 5 μm ODS HPLC column (Hypersil, Jones Chromatography Ltd., Hengoed, UK). The column was fixed within a temperature controlled column oven (Jasco CO-965, Jasco Corp., Japan) set to 40 °C. UV detection of the drug was performed at a wavelength set to 235 nm. Quantification was carried out by an external standard method and linearity was checked between 0.05 and 50 μg/mL for the drug.

2.2.4.2. Preparation of DPI formulation. Binary carrier-based formulations contained 0.8% (w/w) micronised budesonide produced from different primary crystal sources. The drug was blended with lactose monohydrate (Respitose, SV003, DMV-Fonterra Excipients, Vehgel, Netherlands) and had a nominal dose of 200 μg per 25 mg shot weight.

Blends were prepared in glass vials using a geometric blending sequence. Briefly, the weighed drug was placed in between two layers of lactose of approximately the same volume and mixed for 60 s (Whirlimixer, Fisons, Loughborough, UK). Subsequent additions of lactose were added geometrically, with a further 60 s of mixing after each addition. The vial was transferred into a Turbula mixer (Turbula T2F, Willy A Bachofen AG, Basel, Switzerland) and subsequently mixed for a further 45 min. The samples were then stored at 44% RH for 24 h prior to content uniformity determination.

2.2.4.3. Content uniformity. Following blending, ten random samples of 25 ± 1 mg, from different areas of the powder bed, were weighed and dissolved in 50 mL of mobile phase. The amount of drug in each sample was obtained from HPLC assay and the content uniformity expressed as percentage relative standard deviation (%RSD).

2.2.4.4. In vitro aerosol deposition studies. Prepared blends of each material was accurately filled into size 3 HPLC capsules (25 ± 1 mg, QualiV, Qualicaps, bn. E0701921, Madrid, Spain) and stored at 44% RH for 24 h prior to testing. The *in vitro* performance of each formulation was evaluated using a Next Generation Impactor (NGI, Copley Scientific, Nottingham, UK) with pre-separator. The pre-separator was charged with 15 mL mobile phase. Each of the individual stages were coated in 1% silicon oil (Agros Organics, Geel, Belgium) in hexane solution and allowed to air dry. The flow rate of through the impactor was set to 90 L/min using a digital flow meter (DFM2000, Copley Scientific, Nottingham, UK). The formulations were aerosolised from a Cyclohaler (TEVA, Netherlands) over a duration of 2.7 s at 90 L/min. For each repeat ($n = 3$), two capsules were actuated after which the whole system was individually washed down with mobile phase. The capsules, device, mouthpiece and throat were individually washed into volumetric flasks. The pre-separator was removed from the NGI and was showed down into a total volume of 100 mL of mobile phase. The NGI cups were washed down separately using a known amount of mobile phase. An aliquot was then taken from all samples for HPLC analysis. This protocol was repeated three times for each blend, following which, the mass median aerodynamic diameter (MMAD) geometric standard deviation (GSD), fine particle dose less than 5.0 μm (FPD) and fine particle fraction (FPF) were determined. MMAD and GSD were calculated based upon the inverse normals of the cumulative % under the stated aerodynamic diameter *versus* the log of the effective cutoff diameter. Linear regression of the five data points closest to 50% of the cumulative particle mass that entered the cascade impactor was performed to compute the MMAD and GSD.

3. Results and discussion

The relationship between primary crystallisation and secondary micronisation of budesonide using a combination of physicochemical, AFM-nanoindentation and CAB measurements was investigated. The crystallisation of budesonide was conducted using different solvent/anti-solvent conditions, following which the resultant crystals were air-jet micronised. The surface interfacial properties of micronised budesonide produced from two different crystallisation conditions were determined with respect to lactose monohydrate. These data were then compared to the performance of carrier-based DPI formulations containing budesonide produced under different crystallisation conditions.

3.1. Physicochemical characterisation of primary budesonide crystals

The particle size distribution (PSD) analysis of the two primary crystalline sources of budesonide are shown in Table 1. The median diameter of samples A and B were similar, although the span of sample B was broader, therefore suggesting the presence of coarser crystals. Scanning electron microscopy (SEM) micrographs and crystal modelling of the crystalline faces of samples A and B are shown in Fig. 1. SEM images of the samples supported the particle size analysis data with the suggestion of a wider particle size distribution of sample B. Two distinctive crystal morphologies were evident. The crystals produced from acetone (sample A) possessed a diamond like habit, while budesonide crystallised from DMF (sample B) conformed to a more tabular morphology. These images together with the modelling of the crystal habits, suggested the addition of the solvents directly affected the relative growth kinetics of the crystal faces. However, there was no evidence of a new crystalline face being formed. The addition of the anti-solvent to the N,N-dimethylformamide solution of budesonide (sample B), suggested that the slowest growing faces were the {0 0 2}. However, the acetone solution (sample A), under otherwise identical crystallisation conditions, suggested that the {0 1 1} and {1 0 1} faces grew at a lower growth rate than {0 0 2} faces.

Representative DSC thermograms of samples A and B are shown in Fig. 2. For both samples, an endothermic peak was observed at ~260 °C, consistent with previously reported melting temperature of budesonide (Velaga et al., 2002; Jones et al., 2008a). There is however, a suggestion in the DSC thermograms that the melting endotherm for sample B is broader and the onset temperature of melting was observed to be approximately 5° lower for sample B compared to sample A. The melting point of sample A was *ca.* 263 °C and for sample B was *ca.* 260 °C. This lowering in the onset and peak melting temperature may suggest greater levels of impurities or greater levels of disorder in the primary crystals of sample B (Thompson et al., 2004). Endothermic events occurring below

Table 1
Particle size distribution of crystalline budesonide samples A and B.

Sample	d_{10} (μm ± SD)	d_{50} (μm ± SD)	d_{90} (μm ± SD)	Span	VMD (μm ± SD)
Sample A	17.79 ± 0.04	40.13 ± 0.07	62.84 ± 0.20	1.12 ± 0.01	40.40 ± 0.58
Sample B	16.96 ± 0.25	58.72 ± 0.55	95.20 ± 0.90	1.33 ± 0.01	57.87 ± 0.54

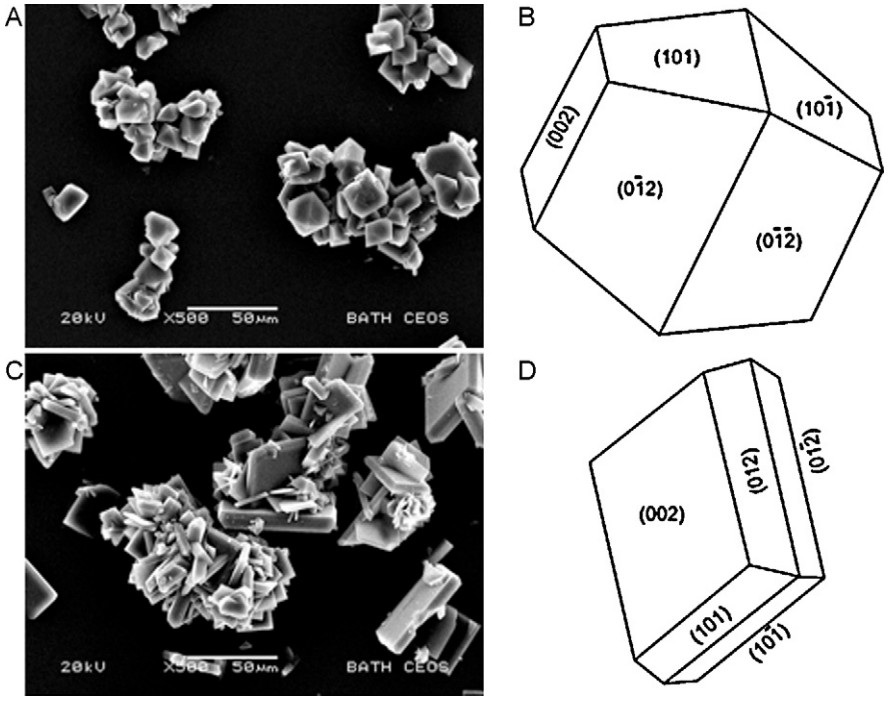

Fig. 1. Scanning electron micrographs and computer models of the crystal habits of sample A (A and B) and sample B (C and D).

100 °C were observed in both samples and may be indicative of the presence of residual solvents within the dried samples.

The XRD patterns of the two samples are shown in Fig. 3. The representative XRD for the two samples displayed similar sharp diffraction peaks at the same two-theta angles, which suggested that the samples were crystalline and exhibited the same polymorphic form. The diffraction patterns for these two batches of budesonide were similar to those reported by Albertsson et al. (1978).

3.2. Mechanical measurements of the primary budesonide crystals

All mechanical measurements were performed on the {0 0 2} faces, particularly as it provided the most accessible face for probe–substrate interaction during force loading experiments, and allowed direct comparison of the influence of the different crystallisation conditions on the Young's modulus. Topographical imaging of the crystal surfaces were recorded before and after each indentation cycle to ensure the suitability of the crystal surface for indentation and to ensure that no plastic deformation had occurred upon loading and unloading.

Representative surface topography images of the {0 0 2} faces of samples A and B before and upon indentation are shown in Fig. 4. The arrows in Fig. 4 indicate the regions where the probe made initial contact with the substrate during tip-substrate engagement, where the high loading stresses being placed on the crystal surface during engagement led to plastic deformation. The additional loading and unloading measurements on the substrate surfaces show no sign of plastic deformation.

A number of representative indentation$^{3/2}$ *versus* loading force plots on different crystal of samples A and B are shown in Fig. 5. These data indicate that the indentation of sample A was significantly greater than that of sample B, suggesting that sample B

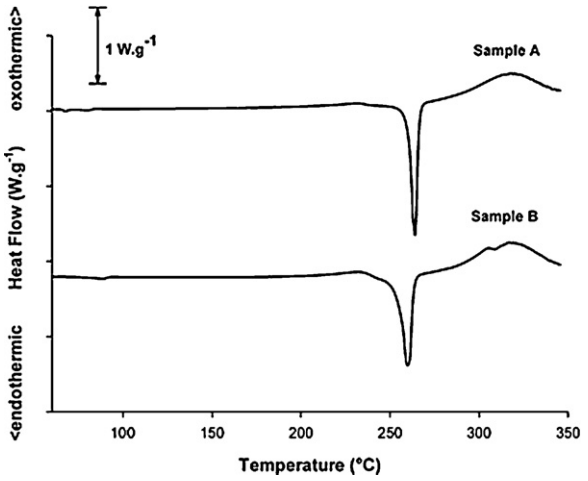

Fig. 2. Representative thermograms of the DSC traces of budesonide samples A and B.

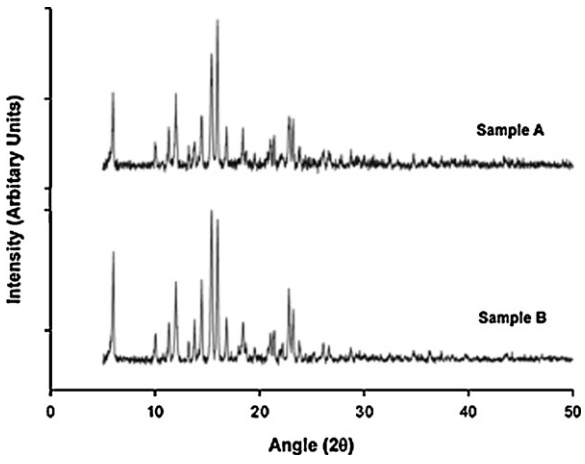

Fig. 3. The X-ray powder diffraction profile of the primary budesonide crystals of samples A and B.

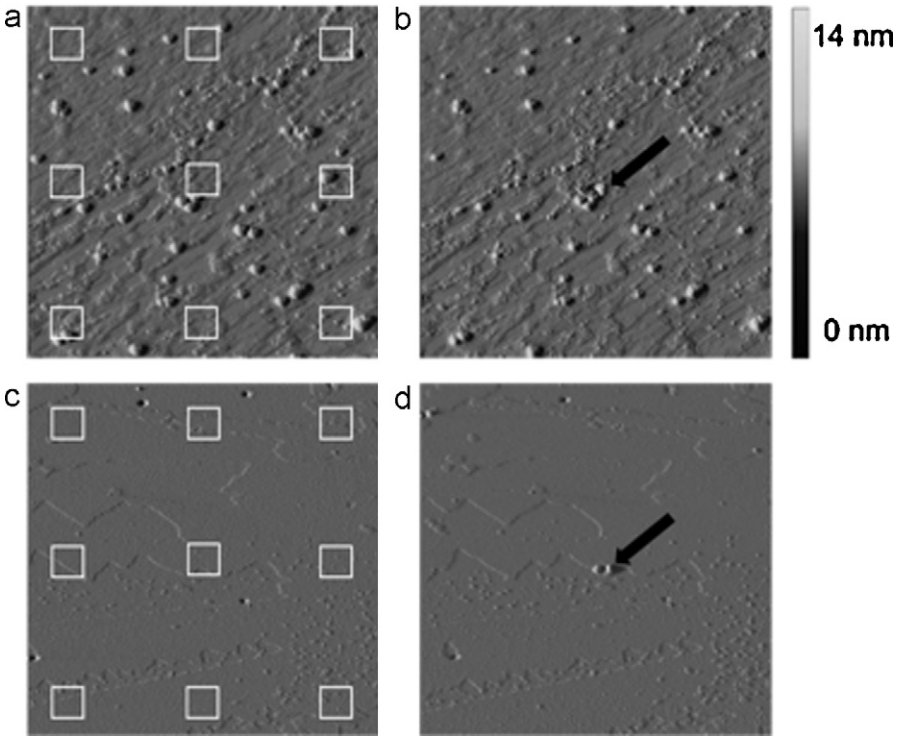

Fig. 4. Atomic force microscope images (3 μm × 3 μm) of sample A before indentation (a), sample A post indentation (b) and sample B prior to indentation (c) and sample B after indentation. The boxes (□) indicate areas where mechanical measurements were undertaken. The black arrows indicate the point of initial contact upon tip–substrate engagement, where high loading has resulted in plastic deformation.

was stiffer, exhibiting a greater resistance to elastic deformation. The gradients of the individual loading *versus* indentation$^{3/2}$ curves were calculated and used to measure the Young's modulus values via the Hertzian model of deformation (Eq. (1)). The Young's modulus measurements for samples A and B are summarised in Table 2.

The Young's modulus of sample B (4.04 ± 1.35 GPa) was significantly higher than sample A (0.95 ± 0.5 GPa, $P < 0.01$), indicating that a change in the solvent environment during primary crystallisation may directly impact the mechanical properties of these materials. These observed variation in Young's modulus and the possible influence of primary crystallisation conditions is further supported by AFM nano-indentation measurement on the (0 0 2) face of budesonide by Davies et al. (2005). They determined that the Young's modulus of unmicronised budesonide was 10 GPa.

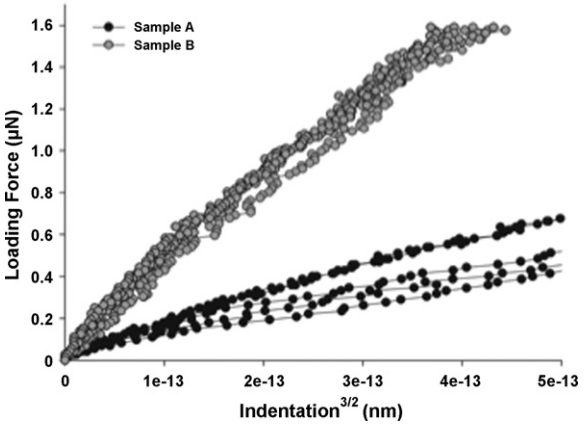

Fig. 5. Individual loading force against the indentation$^{3/2}$ plots for the contact of a hemispherical probe on the {0 0 2} faces of a number of different crystals of samples A and B.

Table 2
The Young's modulus values obtained on the {0 0 2} face of different crystals of samples A and B using AFM nano-indentation. At total of 8 nano-indentation measurements were undertaken on three different crystals of each sample ($n = 24$).

Sample	Young's modulus (GPa ± SD)
Sample A	0.95 ± 0.50
Sample B	4.04 ± 1.35

However, information regarding the crystallisation of these crystals was not known. These range of values suggest that primary crystallisation conditions, which directly influence nucleation kinetics and crystal growth, may directly influence the materials resistance to deformation.

3.3. Effect of crystal habit on secondary processing of budesonide

An air-jet micronisers was employed to reduce the crystalline particles to a respirable size range (less than 5 μm). The micronised batches were investigated for differences in their interfacial interactions using the CAB approach to colloidal probe AFM, and *in vitro* deposition performance upon being blended with a coarse grade of lactose monohydrate.

The particle size distribution (PSD) of the unmicronised and micronised budesonide samples of A and B are shown in Fig. 6 and PSD analysis of the micronised material provided in Table 3. Although the volume median diameter (VMD) and span of the primary crystals of sample A was smaller than sample B, the particle size reduction ratios and span of the respective micronised PSDs were not conserved. The VMD reduction of sample A was 88.7%, which was smaller than that of sample B that had a VMD reduction of 93.8%. The increase in the span of the PSD for sample A, suggests that the efficiency of particle size reduction for sample A was not as efficient as sample B. This observation in the milling behaviour could be related to a change in the crystal morphology, as

Table 3
Particle size distribution analysis of micronised budesonide samples A and B.

Sample	d_{10} (μm ± SD)	d_{50} (μm ± SD)	d_{90} (μm ± SD)	Span (±SD)	VMD (μm ± SD)
Sample A	0.96 ± 0.02	3.38 ± 0.06	8.02 ± 0.01	2.11 ± 0.05	4.18 ± 0.09
Sample B	0.95 ± 0.02	3.14 ± 0.05	6.90 ± 0.03	1.90 ± 0.03	3.59 ± 0.04

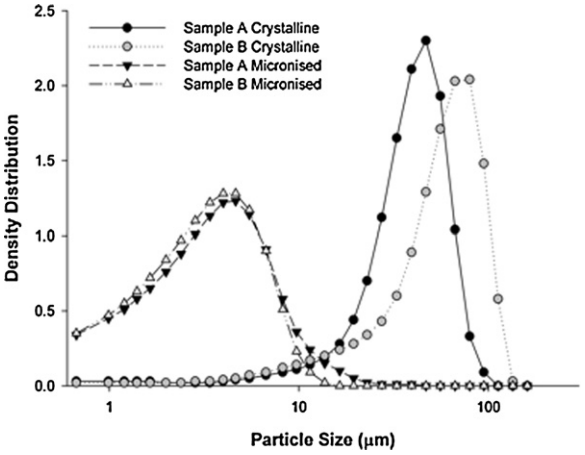

Fig. 6. Particle size distribution of the unmicronised (primary crystals) and micronised (secondary) samples of budesonide.

highlighted by the study of adipic acid (Chikhalia et al., 2006), which may expose crystalline faces that can be fractured more effectively, or that the increase in the Young's modulus of sample B may have a contributing factor to the efficiency of particle size reduction.

The CAB data of the two micronised budesonide samples with respect to their interactions with the {0 0 2} faces of their respective unmicronised forms and lactose monohydrate are shown plotted in Fig. 7. The CAB measurements of the micronised particles were 0.728 ± 0.020 (R^2 = 0.9970) and 0.578 ± 0.010 (R^2 = 0.9980) for samples A and B, respectively. The CAB value of sample B was similar to previously reported CAB measurements of commercially supplied micronised budesonide of 0.543 with respect to lactose monohydrate (Hooton et al., 2008). Hooton et al. had shown by crystal modelling that the surface chemistry of the {0 0 2} face was hydrophobic and therefore, would only be able to adhere via apolar-based interactions. Hence, this may explain the greater adhesion of micronised budesonide samples in the present study to lactose than the corresponding force of cohesion measured against the {0 0 2} face budesonide. Further analysis suggests that for an equivalent force of cohesion the adhesion of the micronised particles from sample B to lactose was approximately 22% greater than particles from sample A. These data suggest that greater deaggregation

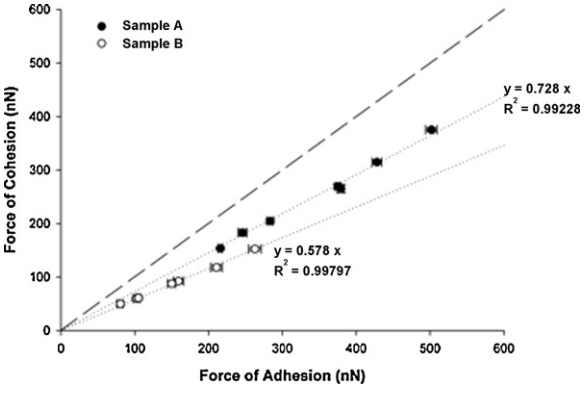

Fig. 7. CAB plots for micronised samples A and B of budesonide with respect to lactose.

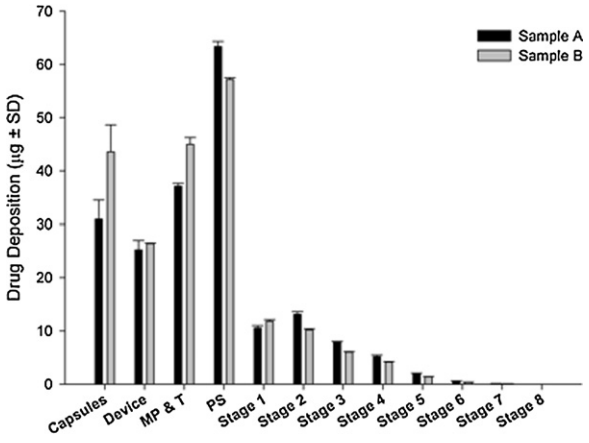

Fig. 8. NGI stage-by-stage deposition profile of budesonide samples A and B.

energy may therefore be required to elutriate the respirable sized particles of sample B from a lactose monohydrate surface.

The content uniformity of each formulation was evaluated prior to impaction testing and is expressed as a percentage relative standard deviation (%RSD). These were determined to be 1.72% and 1.03% for samples A and B respectively, suggesting homogeneous distribution of the API throughout the formulation blend. Given that these values were lower than 5%, both formulations were deemed suitable for *in vitro* impaction testing.

The *in vitro* aerosolisation performance of carrier based DPI formulations containing samples A and B was assessed using a next generation impactor (NGI). Drug deposition profiles of both formulations within the NGI are shown in Fig. 8. In addition, the emitted dose (ED), FPD and FPF data are summarised in Table 4.

The emitted dose of DPI formulations containing either sample A or sample B were 164.1 ± 1.4 and 161.8 ± 1.6, respectively. These data show that the emitted dose from formulations containing either API were similar (Table 4). The FPD and % FPF of budesonide upon aerosolization of the formulation containing sample A was 15.9 ± 0.4 μg and 9.7 ± 0.3%, respectively. In contrast, the performance of DPI formulations containing budesonide sample B, as measured by the FPD and % FPF, was 11.7 ± 0.3 μg and 7.2 ± 0.1%, respectively. The impactor deposition profiles of samples A and B upon aerosolisation from the cyclohaler device showed a significant increase in the mass deposited in the lower stages of the impactor for budesonide sample A (ANOVA, $P < 0.05$) in comparison to sample B, which is supported by the significantly (ANOVA, $P < 0.05$) greater % FPF of budesonide sample A than sample B (Table 4).

The aerosolisation performance of carrier-based formulations are significantly influenced by the interfacial forces of interaction between the API and carrier (Begat et al., 2004b; Hooton

Table 4
In vitro performance characteristics of the two samples of budesonide using NGI testing (FPF_{ED}, fine particle fraction of the emitted dose).

	Sample A	Sample B
Emitted dose (μg ± SD)	164.1 (1.4)	161.8 (1.6)
Fine particle dose (μg ± SD)	15.9 (0.4)	11.7 (0.3)
FPF_{ED} (% ± SD)	9.7 (0.3)	7.2 (0.1)

et al., 2006; Jones et al., 2008b). Analysis of the surface interfacial properties of budesonide samples A and B suggested that sample B had a greater adhesive affinity to lactose than sample A. The greater adhesive tendency of sample B to lactose, therefore, may have contributed to the materials lower deaggregation efficiency in comparison to sample A. These data, therefore, highlight the relationship between mechanical properties of the different samples of primary budesonide crystals and their micronisation behaviour, particle size reduction properties, interfacial properties and *in vitro* performance in carrier-based DPI formulations.

4. Conclusion

This study has demonstrated the importance of understanding the implications of modifying the crystal habit for budesonide included in carrier-based DPI formulations. The use of different crystallisation conditions has led to significant differences in the mechanical properties of the primary crystalline material and altered the CAB value of the micronised materials. In turn, these differences are suggested to influence the *in vitro* performance of DPI formulations. This work highlighted the effect and implications resulting from changes in the primary crystallisation of APIs and advocates careful consideration when developing crystallisation processes for these materials.

Acknowledgement

Financial support for this project was provided by the Engineering and Physical Sciences Research Council (EPSRC).

References

Abu Bakar, M.R., Nagy, Z.K., Saleemi, A.N., Rielly, C.D., 2009. The impact of direct nucleation control on crystal size distribution in pharmaceutical crystallization processes. Cryst. Growth Des. 9, 1378–1384.

Albertsson, J., Oskarsson, Å., Svensson, C., 1978. X-ray study of budesonide: molecular structures and solid solutions of the (22S) and (22R) epimers of 11β,21-dihydroxy-16α,17α-propylmethylenedioxy-1,4-pregnadiene-3,20-dione. Acta Crystallogr. B: Struct. Crystallogr. Cryst. Chem. 34, 3027–3036.

Banga, S., Chawla, G., Varandani, D., Mehta, B.R., Bansal, A.K., 2007. Modification of the crystal habit of celecoxib for improved processability. J. Pharm. Pharmacol. 59, 29–39.

Beach, S., Latham, D., Sidgwick, C., Hanna, M., York, P., 1999. Control of the physical form of salmeterol xinofoate. Org. Process Res. Dev. 3, 370–376.

Begat, P., Young, P., Edge, S., Kaerger, J., Price, R., 2003. The effect of mechanical processing on surface stability of pharmaceutical powders: visualization by atomic force microscopy. J. Pharm. Sci. 92, 611–620.

Begat, P., Morton, D., Staniforth, J., Price, R., 2004a. The cohesive–adhesive balances in dry powder inhaler formulations. I. Direct quantification by atomic force microscopy. Pharm. Res. 21, 1591–1597.

Begat, P., Morton, D., Staniforth, J., Price, R., 2004b. The cohesive–adhesive balances in dry powder inhaler formulations. II. Influence on fine particle delivery characteristics. Pharm. Res. 21, 1826–1833.

Brodka-Pfeiffer, K., Langguth, P., Grass, P., Hausler, H., 2003. Influence of mechanical activation on the physical stability of salbutamol sulphate. Eur. J. Pharm. Biopharm. 56, 393–400.

Chikhalia, V., Forbes, R., Storey, R., Ticehurst, M., 2006. The effect of crystal morphology and mill type on milling induced crystal disorder. Eur. J. Pharm. Sci. 27, 19–26.

Davies, M., Brindley, A., Chen, X., Marlow, M., Doughty, S., Shrubb, I., Roberts, C., 2005. Characterization of drug particle surface energetics and Young's modulus by atomic force microscopy and inverse gas chromatography. Pharm. Res. 22, 1158–1166.

de Vegt, O., Vromans, H., den Toonder, J., van der Voort Maarschalk, K., 2009. Influence of flaws and crystal properties on particle fracture in a jet mill. Powder Technol. 191, 72–77.

Fraxedas, J., Garcia-Manyes, S., Gorostiza, P., Sanz, F., 2002. Nanoindentation: toward the sensing of atomic interaction. Proc. Natl. Acad. Sci. U.S.A. 99, 5228–5232.

Garekani, H., Sadeghi, F., Badiee, A., Mostafa, S., Rajabi-Siahboomi, A., 2001. Crystal habit modifications of ibuprofen and their physicomechanical characteristics. Drug Dev. Ind. Pharm. 27, 803–809.

Hertz, H., 1881. Ueber die Berührung fester elastischer Körper (on the contact of elastic solids). J. Reine Angew. Math. 92, 156–171.

Hooton, J.C., German, C.S., Allen, S., Davies, M.C., Roberts, C.J., Tendler, S.J.B., Williams, P.M., 2004. An atomic force microscopy study of the effect of nanoscale contact geometry and surface chemistry on the adhesion of pharmaceutical particles. Pharm. Res. 21, 953–961.

Hooton, J.C., Jones, M.D., Price, R., 2006. Predicting the behavior of novel sugar carriers for dry powder inhaler formulations via the use of a cohesive–adhesive force balance approach. J. Pharm. Sci. 95, 1288–1297.

Hooton, J.C., Jones, M.D., Harris, H., Shur, J., Price, R., 2008. The influence of crystal habit on the prediction of dry powder inhalation formulation performance using the cohesive–adhesive force balance approach. Drug Dev. Ind. Pharm. 34, 974–983.

Hutter, J., Bechhoefer, J., 1993. Calibration of atomic force microscope tips. Rev. Sci. Instrum. 64, 1868–1873.

Hüttenrauch, R., Fricke, S., Zielke, P., 1985. Mechanical activation of pharmaceutical systems. Pharm. Res. 2, 302–306.

Jones, M.D., Young, P.M., Traini, D., Shur, J., Edge, S., Price, R., 2008a. The use of atomic force microscopy to study the conditioning of micronised budesonide. Int. J. Pharm. 357, 314–317.

Jones, M.D., Harris, H., Hooton, J.C., Shur, J., King, G.S., Mathoulin, C.A., Nichol, K., Smith, T.L., Dawson, M.L., Smith, T.L., Dawson, M.L., Ferrie, A.R., Price, R., 2008b. An investigation into the relationship between carrier-based dry powder inhalation performance and formulation cohesive–adhesive force balances. Eur. J. Pharm. Biopharm. 69, 496–507.

Liao, X., Wiedmann, T., 2004. Characterization of pharmaceutical solids by scanning probe microscopy. J. Pharm. Sci. 93, 2250–2258.

Murnane, D., Marriott, C., Martin, G.P., 2008. Crystallization and crystallinity of fluticasone propionate. Cryst. Growth Des. 8, 2753–2764.

Murnane, D., Martin, G.P., Marriott, C., 2009. Dry powder formulations for inhalation of fluticasone propionate and salmeterol xinafoate microcrystals. J. Pharm. Sci. 98, 503–515.

Muster, T.H., Prestidge, C.A., 2002. Face specific surface properties of pharmaceutical crystals. J. Pharm. Sci. 91, 1432–1444.

Newman, S., 2002. Evolution of dry powder inhaler design, formulation, and performance. Respir. Med. 96, 293–304.

Perkins, M.C., Bunker, M., James, J., Rigby-Singleton, S., Ledru, J., Madden-Smith, C., Luk, S., Patel, N., Roberts, C.J., 2009. Towards the understanding and prediction of material changes during micronisation using atomic force microscopy. Eur. J. Pharm. Sci. 38, 1–8.

Perkins, M., Ebbens, S.J., Hayes, S., Roberts, C.J., Madden, C.E., Luk, S.Y., Patel, N., 2007. Elastic modulus measurements from individual lactose particles using atomic force microscopy. Int. J. Pharm. 332, 168–175.

Plassard, C., Lesniewska, E., Pochard, I., Nonat, A., 2004. Investigation of the surface structure and elastic properties of calcium silicate hydrates at the nanoscale. Ultramicroscopy 100, 331–338.

Sader, J.E., Larson, I., Mulvaney, P., White, L.R., 1995. Method for the calibration of atomic force microscope cantilevers. Rev. Sci. Instrum. 66, 3789.

Taylor, L., Papadopoulos, D., Dunn, P., Bentham, A., Mitchell, J., Snowden, M., 2004. Mechanical characterisation of powders using nanoindentation. Powder Technol. 143, 179–185.

Telko, M.J., Hickey, A.J., 2005. Dry powder inhaler formulation. Respir. Care 50, 1209–1227.

Thompson, C., Davies, M.C., Roberts, C.J., Tendler, S.J.B., Wilkinson, M.J., 2004. The effects of additives on the growth and morphology of paracetamol (acetaminophen) crystals. Int. J. Pharm. 280, 137–150.

Timsina, M., Martin, G., Marriott, C., Ganderton, D., Yianneskis, M., 1994. Drug-delivery to the respiratory-tract using dry powder inhalers. Int J. Pharm. 101, 1–13.

Velaga, S., Berger, R., Carlfors, J., 2002. Supercritical fluids crystallization of budesonide and flunisolide. Pharm. Res. 19, 1564–1571.

Willart, J.F., Descamps, M., 2008. Solid state amorphization of pharmaceuticals. Mol. Pharm. 5, 905–920.

Wood, W., 2001. A bad (crystal) habit – and how it was overcome. Powder Technol. 121, 53–59.

Young, P.M., Tobyn, M.J., Price, R., Buttrum, M., Dey, F., 2006. The use of colloid probe microscopy to predict aerosolization performance in dry powder inhalers: AFM and in vitro correlation. J. Pharm. Sci. 95, 1800–1809.

Zugner, S., Marquardt, K., Zimmermann, I., 2006. Influence of nanomechanical crystal properties on the comminution process of particulate solids in spiral jet mills. Eur. J. Pharm. Biopharm. 62, 194–201.